# CSEM FOR $CO_2$ STORAGE – FEASIBILITY STUDY AT SMEAHEIA TO OPTIMISE ACQUISITION

**Romina Gehrmann[1], Anouar Romdhane[2], Joonsang Park[3], Peder Eliasson[2]**

[1] University of Southampton, Southampton, UK

[2] SINTEF, Trondheim, Norway

[3] NGI, Oslo, Norway

* Corresponding author e-mail: r.a.gehrmann@soton.ac.uk

## Abstract

In this work, we evaluate the use of controlled-source electromagnetics (CSEM) for $CO_2$ monitoring at Smeaheia, a possible candidate for future phases of the Norwegian full-scale CCS project. CSEM is sensitive to electrically resistive material replacing conductive pore water in the pore space, which enables to infer volumetric estimates of the injected $CO_2$ in the formation. CSEM is often used in combination with high-resolution seismic reflection data due to the sensitivity of the two methods to complementary physical properties. Here, we present a technique to optimise the CSEM survey parameters for efficient 4D surveying. Realistic synthetic models prior to and after injection are derived from reservoir modelling and converted to electrical resistivities. Inversion tests are carried out in 2D for the baseline and monitor cases considering realistic data errors. We show that the resistivity changes due to $CO_2$ injection can be monitored using CSEM. We discuss the optimal orientation of the receivers, frequency range and transmitter-receiver offset. We finally discuss a strategy for optimal survey design based on the sensitivity to the $CO_2$ plume.

***Keywords:*** *$CO_2$ storage, Smeaheia, CSEM, acquisition design*

## 1. Introduction

An accurate and efficient monitoring strategy is essential for safe $CO_2$ storage in compliance with laws and regulations. The reliability of monitoring technology is also crucial for the public acceptance of CCS, especially in case of large-scale storage and import of $CO_2$ from other countries. The cost of a comprehensive monitoring program, covering the different phases of a storage project, however, could quickly become prohibitively high, if not carefully optimised. In this context, geophysical monitoring methods play a key role in any proposed measurement, monitoring, and verification (MMV) plan aiming to derive, from measured data, estimates of the spatial distribution of selected physical properties of the subsurface.

While seismic surveys will most likely be the backbone of any $CO_2$ storage geophysical monitoring program, controlled-source electromagnetics (CSEM) can be a valuable complement. By providing an additional, yet essential, earth parameter (electrical resistivity), CSEM contributes to significantly better-constrained estimates of the pressure and saturation changes caused by $CO_2$ injection, and mitigates uncertainties in seismic data interpretation. The improved capability of quantitative characterisation by combining seismic and CSEM will therefore reduce risks and support the development of better tailored, sparser (in time and space) geophysical surveys and will consequently help to reduce costs.

The resolution of CSEM is inherently lower than that of seismic and therefore resolution capabilities, time-lapse approaches, and optimum ways of combining seismic and CSEM data should be carefully investigated. Time-lapse CSEM has not been used frequently in the past for $CO_2$ storage or hydrocarbon monitoring. While several synthetic studies have concluded that time-lapse changes are detectable and resolvable (e.g., Colombo and McNeice, 2013), acquisition must be done very carefully to achieve sufficient repeatability (Tietze et al., 2018). Several publications have investigated the sensitivity to production-induced reservoir changes, e.g., movement of the injected waterfront (e.g., Lien and Mannseth, 2008; Orange et al., 2009; Zach et al., 2009). They have shown that CSEM monitoring is feasible, i.e., the responses from production-induced changes in hydrocarbon saturation exceed the measurement uncertainty, at least for simple models of the evolving fluid distribution. However, the feasibility of time-lapse CSEM in realistic 3D reservoir geometry (e.g., based on seismic interpreted structure) has not been fully considered. Also, realistic, highly spatially variable small-scale changes of subsurface resistivity due to $CO_2$ injection have not been studied (Streich, 2016).

The use of CSEM imaging for onshore $CO_2$ sequestration sites has been evaluated in some studies (Grayver et al., 2014). Experience with marine CSEM for $CO_2$ sequestration monitoring, however, is very limited, and restricted to simple feasibility studies (Park et al., 2019; Shantsev et al., 2020, Morten and Bjørke, 2020) and a case study at Sleipner (e.g., Bøe et al., 2017) using real data monitor vintage.

Large research efforts have been made during the last decades to improve solving large-scale non-linear

problems. This has resulted in CSEM inversion becoming tractable in 3D (e.g., Amaya et al., 2016; Patzer et al., 2017). Much less attention is, however, given to survey design strategies which conceptually aims at selecting the data acquisition that optimally resolve the subsurface model parameters (accuracy/resolution) of interest. Standard procedures are often suggested, and data redundancy considered to mitigate issues related to data inadequacy, but may result in unnecessary additional costs. In this context, experimental design can be used to find the best trade-off between data value and data collection cost. An overview of the techniques that can be used is provided in Maurer et al., 2010. Examples of applications to electromagnetics surveying are given in Maurer et al., 2000, Roux and Garcia, 2014, and Romdhane and Eliasson, 2018.

In this work, we evaluate the use of CSEM for $CO_2$ monitoring at Smeaheia, a possible candidate for future phases of the Norwegian full-scale CCS project and analyse ways to optimise the survey design. In a first stage, the paper introduces the techniques used for CSEM inversion and for the acquisition design optimisation. The results from the synthetic study at Smeaheia are then described for the baseline and monitoring case (25 years after injection). Finally, the results from the optimal survey design analysis are presented and discussed in regard to electric field components, spatial distribution of instrumentation and signal frequency content.

## 2. Methodology

This section briefly describes the algorithm used for CSEM inversion and for the acquisition design analysis.

### *2.1 CSEM inversion*

The code used to invert the synthetic data for this study is the freely available modelling and inversion MARE2DEM software that can model magnetotelluric and CSEM data in frequency domain and incorporate anisotropic resistivity models (Key, 2016). The forward modelling is performed in 2.5-D (Key and Ovall, 2011) and adaptively refines the forward modelling grid for an optimum accuracy. The inversion is based on the Occam minimisation algorithm (Constable et al., 1987) with possibilities for incorporating available prior information and regularisation. The misfit function being minimised can be written as:

$$U = ||\mathbf{Rm}||2 + ||\mathbf{P}(\mathbf{m}-\mathbf{m}^*)||^2 + \mu^{-1}||\mathbf{W}(\mathbf{d}_{obs} - \mathbf{d}_{cal})||^2$$

where $\mathbf{m}$ is the model parameter vector for $\log_{10}$(resistivity) values, $\mathbf{m}^*$ is the prior model vector describing available prior information which can be weighted with the non-zero diagonal values in $\mathbf{P}$. The diagonal matrix $\mathbf{W}$ contains the inverse standard errors for the observed data $\mathbf{d}_{obs}$. The data fit (last term) is the difference of the observed to the calculated data $\mathbf{d}_{cal}$ divided by their respective errors squared. $\mathbf{R}$ denotes the model roughness regularisation. The Lagrange multiplier $\mu$ is used to trade-off the data fit against the other two terms and is optimised automatically during the inversion.

### *2.2 Acquisition design*

We quantify the quality of a given acquisition layout through the computation of the eigenvalue spectrum of the approximate Hessian on a defined target region.

The approximate Hessian can be defined as:

$$\boldsymbol{H_a} = \Re\{\mathbf{J}^T \boldsymbol{C_d} \mathbf{J}^*\}$$

Where $\Re$ denotes the real part of a complex number. The superscripts $T$ and * correspond to the ordinary matrix transpose and complex conjugate, respectively. $\boldsymbol{C_d}$ is the data covariance matrix describing data uncertainties. $\mathbf{J}$ is the Jacobian or sensitivity matrix including spatial derivatives which can be defined as:

$$\mathbf{J} = \frac{\partial \mathbf{d}_{cal}}{\partial \mathbf{m}}.$$

To efficiently compute the eigenvalue spectrum of the approximate Hessian, randomised SVD can be used following the approach described in Halko et al., 2011 and Eliasson and Romdhane, 2017. General sensitivity in the dipole transmitter/receiver domain to changes in the model space can be performed in a selected target (Romdhane and Eliasson, 2018) which can be derived from reservoir modelling. In a $CO_2$ storage context, the target would correspond to the spatial evolution of the plume within the storage reservoir. The spectra corresponding to a selected data trace can then be analysed and compared to the reference spectrum (Maurer et al., 2010).

## 3. Smeaheia case study

### *3.1 Geology and injection scenario*

A feasibility report on a full-scale CCS project in Norway (Gassnova, 2016) suggests the Smeaheia site, which is a fault block located east of the Troll gas field, north-west of Bergen, as one of the most viable storages in the Horda platform (Figure 1).

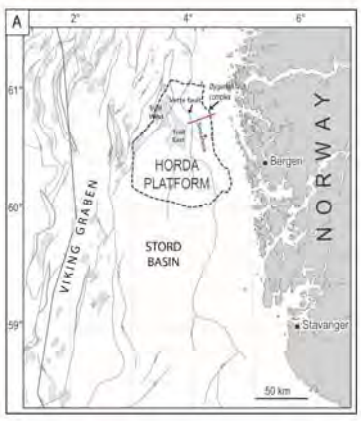


*Figure 1: Location of the Smeaheia site. The red line depicts the location of the CSEM profile used in this study (modified from Dupuy et al., 2018).*

Significant efforts in research and development targeting a better characterisation and monitoring concepts for

Smeaheia are conducted, since the site is considered a good candidate for future phases of the full-scale CCS.

The reservoir in Smeaheia consists of the Sognefjord, Krossfjord, and Fensfjord formations, which are well known in relation to the neighbouring Troll gas-producing field. The $CO_2$ injection is recommended to be done at 1200 to 1500 m depth in the Alpha structure located East of the Vette fault complex (Figure 1). More geological description of the reservoir is available in Dupuy et al., 2018.

### *3.2 Resistivity models*

A reservoir modelling study carried out by the Northern Lights consortium considered the injection scenario in the Alpha structure with a $CO_2$ injection rate of 1.3 Mt/year for 25 years. In this injection scenario, both Vette and Øygarden faults are assumed to be sealing (no fault transmissibility), although this has been identified as a source of uncertainties at Smeaheia (Lothe et al. 2018; Mulrooney et al., 2020). The derived pressure and saturation maps can be used to build synthetic dynamic geophysical models describing key properties like elastic properties or resistivities. In our study, the saturation changes (see example in Figure 2) are converted to resistivity changes using Archie's relationship (Archie, 1942) with a saturation exponent equal to 2 and available information from CSEM survey data in the same area (Park et al., 2019).

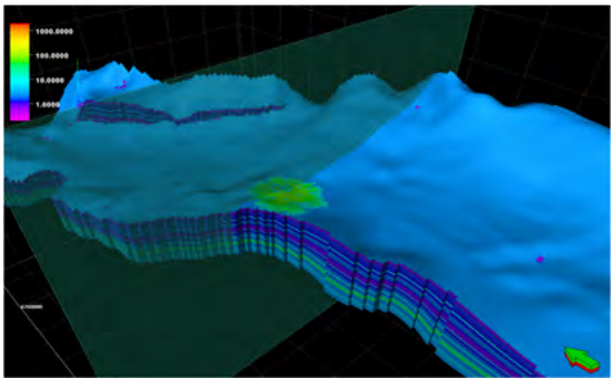

Figure 2: Reservoir saturation model after 25 years of injection (Park et al., 2019).

The resulting 2D resistivity models for the baseline (i.e., before any injection) and after 25 years of injection are displayed in Figure 3, with the effect of the $CO_2$ plume being observed as an increase of resistivity. The plume has a varying thickness between 10 and 50 m and a lateral extent of about 3000 m. These models are used to generate the reference data for the synthetic study.

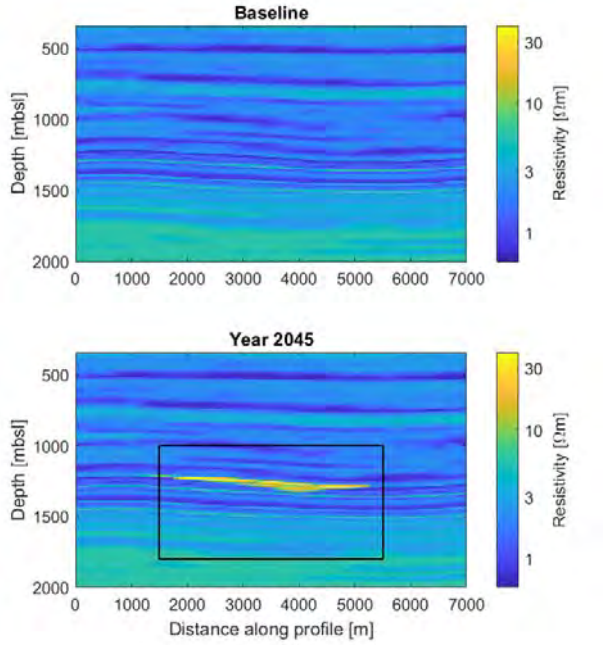


Figure 3: (Top): Baseline resistivity model. (Bottom): Resistivity model after 25 years of injection. Rectangle outlines the targeted area for the acquisition optimisation (section 3.4).

### *3.3 CSEM synthetic study*

#### *3.3.1. Forward modelling and data errors estimate*

To generate the reference data for the baseline and monitor cases, we consider a similar acquisition layout to the one used in Park et al., 2019. A horizontal electric dipole transmitter is towed at 30 m above the seabed with a regular spacing of 300 m, resulting in 41 transmitter positions. The signal is measured using 17 dipole receivers recording the horizontal (in line with the transmitter) and vertical electric fields. The receivers are positioned at the seabed with a spacing of 500 m. The modelled frequencies correspond to 0.1, 0.25, 0.5, 0.75, 1, 2, 3, 4, and 5 Hz. An example of the modelled data is shown in Figure 4.

At a first glance, the amplitude and phase data show sensitivity to the increased resistivity in the reservoir layer. The phase data are relatively more sensitive with several degrees difference between the observed and modelled data. The amplitude data show differences up to two magnitudes smaller than the actual data. The detectability will depend on the size of the data error as well. We therefore perform a data error analysis by perturbing navigational parameters (e.g., Gehrmann et al. 2019) including:

- transmitter and receiver azimuth errors with an error value corresponding to 3°,
- errors (3 m) due to the transmitter depth and transmitter dip (3°), and
- errors for dipole receiver positions along the x and y directions (3 m).

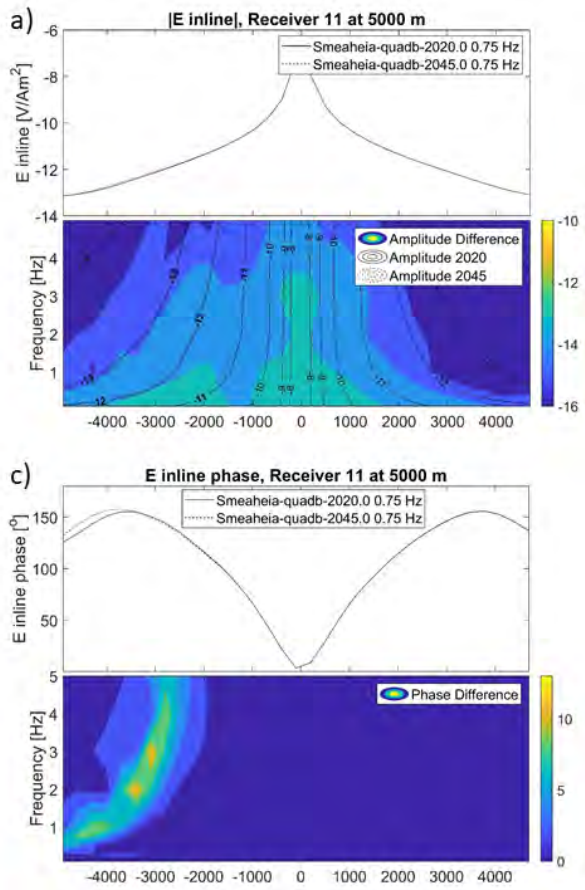


*Figure 4: Synthetic data for inline electric field amplitude (a) and phase (c) for 0.75 Hz for baseline model (solid line) and model after 25 years of injection (dotted line). Data difference over frequency and transmitter-receiver offset with contours for amplitude data. Amplitude is on a logarithmic scale.*

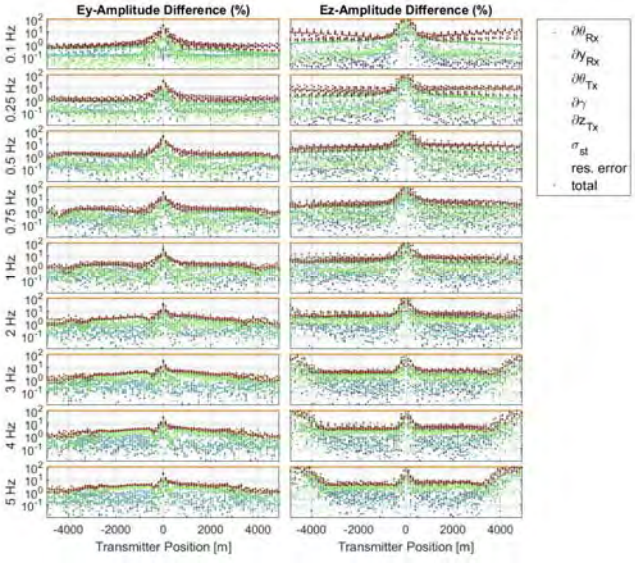


*Figure 5: Data error analysis for transmitter position relative to all receivers at position 0. The total error (red) is the result of the summation of all individual data differences for each perturbation in quadrature. Perturbations are done for azimuth Θ and dip γ and variation in x, y and z for the transmitter (Tx) or receiver (Rx).*

Forward modelling is performed for each perturbation and the total error is derived by adding data difference in quadrature. Figure 5 shows the individual data anomaly resulting from the difference between the cases without and with navigation perturbations. Differences for the inline (Ey) and for the vertical component (Ez) are considered. The differences are displayed in percentage (%) for the amplitude and show that the fields are most sensitive to the lateral position of the receivers and vertical position of the transmitter.

### *3.2.2. Inversion results*

In a first stage, we run the inversion with the baseline data. We add noise based on the navigation error estimates from the previous section assuming a Gaussian distribution. The starting model for the inversion contains a water layer with fixed resistivity of 0.3 Ωm and a homogeneous half space with a resistivity of 1 Ωm. Individual inversions for the inline (Ey) and vertical (Ez) components (Figure 6) converge to root mean squared (rms) misfit values of 1.1 and 1.3 respectively, possibly not reaching the target misfit of 1 due to the data errors being too small when compared to the numerical noise. Both data sets are sensitive to the vertical structure.

The inversion for both components using 14 iterations results in rms misfit of 1.2. The recovered resistivity model (Figure 7a) revealed sensitivity to the alternating conductive and resistive layers but with less vertical resolution than the true model. The first resistive layer is resolved, while the two thin conductive layers in ~500 and ~700 m depth are resolved as one layer in the inversion. Especially with greater depth the inversion tends to resolve one thick layer instead of several thin ones, which is due to the roughness regularisation preventing large resistivity contrasts when the data loses resolution with depth. Data residuals are random and Gaussian distributed (Figure 8).

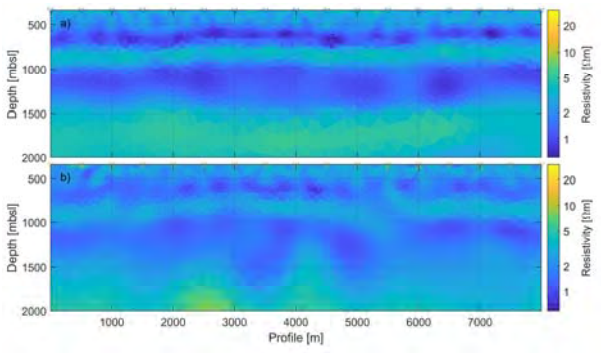


Figure 6: Baseline model inferred from CSEM inversion using (a) inline (Ey) and (b) vertical (Ez) components of the electric field.

In a second stage, we run the inversion with monitor data. We adopted a sequential time-lapse strategy where the resistivity model from the inversion of the baseline data is used as starting model for the inversion of the monitor data. The inversion parameters are the same as for the baseline case. The recovered resistivity model is displayed together with the reference model for comparison in Figure 7b. Updates compared to the result from the baseline inversion can be observed, especially

an increase of resistivity at depth between 1300 and 1600 m (Figure 7c). The observed resistivity increase is located slightly below the true target location. Such deviation can be attributed to the smoothing regularisation.

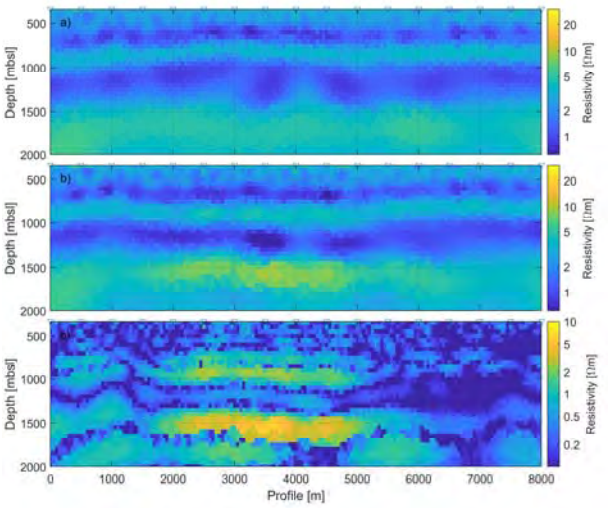


Figure 7: (a) Resistivity model inferred from CSEM inversion using inline and vertical components of the electric field for the baseline case; (b) for the monitor case, 25 years later; (c) Difference between the resistivity model in a and b.

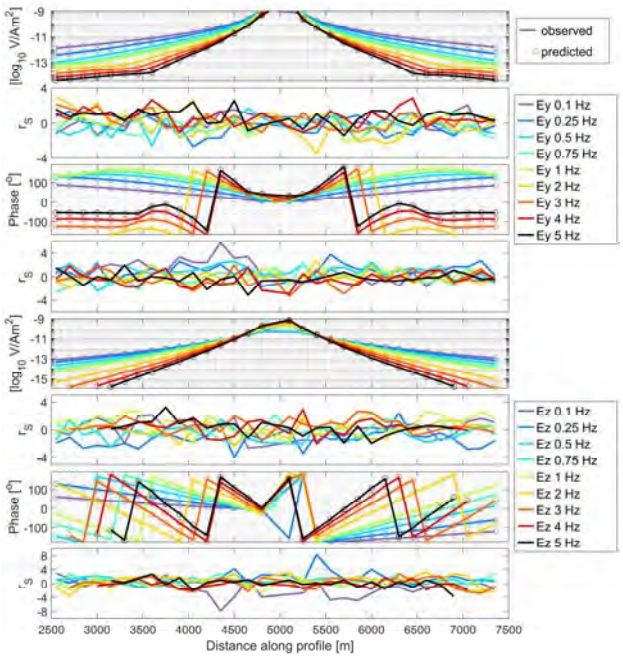


*Figure 8: Amplitude and phase data for the inline (top four panels) and vertical (bottom four panels) component as well as standardised residuals (rs) for final resistivity model shown in Figure 7a*

### *3.3 Acquisition design*

After showing that the CSEM inversion can detect a resistivity change in the expected area, using all available transmitters, receivers, data components, and frequencies, we turn to the investigation of acquisition design. Data components here refer to inline or vertical components and amplitudes or phases. Following the eigenvalue spectrum approach described in Section 2.2, we identify the parts of the CSEM data containing most information for inversion of model parameters in a target region with lateral extension from 1500-5500 m and a depth range from 1000-1800 m, cf. Figure 3. The first selected data trace (transmitter-receiver pair for a specific frequency and data component) is the one that is most sensitive to resistivity changes in the target area, consequently offering the best possibilities to constrain/determine the target area properties during inversion. New traces are then selected iteratively based on how much additional information they bring to the previous traces. For the preliminary Smeaheia study described here, only 50 measurements are selected. This is a tiny fraction of more than 17000 used for the inversion described in Section 3.2. Visual inspection of the eigenvalue spectrum showed that the information content in this small subset of traces is, not surprisingly, smaller than in the full data set. However, an impressive amount of information is captured using those few traces, and they are, for example, shown to provide more information than 500 randomly picked traces (an otherwise often efficient way of decimating data with relatively little loss).

While future work will study in detail how the inversion result itself is affected by using smaller, but optimised, surveys, we present here instead a few examples of what is considered optimal using the described strategy. Figure 9 illustrates how the selected transmitter-receiver pairs always have a certain minimum offset (no markers along the diagonal). The traces are predominantly based on the phase of the electric field (more circles than squares). Lower frequencies are preferred, especially 0.1 Hz.

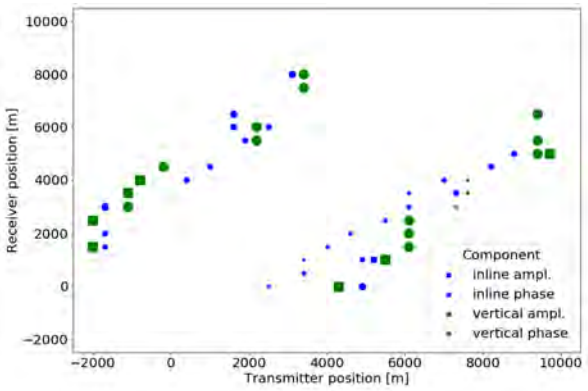


*Figure 9: Illustration of 50 selected optimal data traces using a survey design strategy based on eigenvalue spectrum analysis. The axes of the plot refer to the inline positions of transmitter-receiver pairs. The color indicates whether the inline (blue) or vertical (green) electric field has been chosen, and the shape whether the amplitude (square) or phase (circle) is used. In addition, the size of the markers represents different transmitter frequencies (from 0.1-5 Hz). Larger markers denote lower frequencies.*

The preference of lower frequencies becomes even clearer when plotting offset vs frequency, see Figure 10. This figure also shows an interesting trend in that the

lower frequencies in general are associated with longer offsets, while the selected higher frequencies are associated to pairs with small offsets. This is intuitively a good choice, since the lower frequencies have larger penetration depths. This figure also shows that in general favoured offsets range from 2.5-5 km, which is about twice the depth of the target.

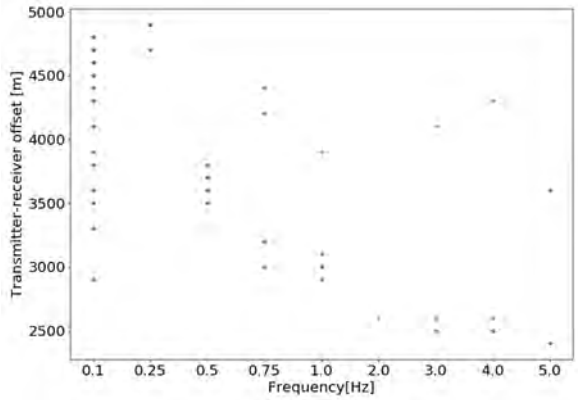


Figure 10: Transmitter-receiver offset vs frequency for 50 data traces identified using survey optimisation based on eigenvalue spectrum analysis.

## Conclusions

In this work, we evaluate the use of CSEM for $CO_2$ monitoring at Smeaheia, a possible candidate for future phases of the Norwegian full-scale CCS project. Realistic synthetic models prior to and after 25 years of injection are derived from reservoir modelling and converted to resistivities. A CSEM time-lapse feasibility study is carried out showing the sensitivity of both vertical and horizontal electric field dipoles to resistivity changes due to $CO_2$ injection. The optimal acquisition analysis reveals the highest sensitivity to the storage region at 1200 m depth for transmitter-receiver offsets between 2500 and 5000 m. When considering electric field components, phase data contain more information than amplitude, which emphasises the requirement for accurate time logging during surveying. The chosen frequency range between 0.1 to 5 Hz is sensitive to the target area, but lower frequencies are preferred, especially for long offsets. Our work illustrates the benefit of an optimal survey design study using realistic subsurface models as a prerequisite for efficient time-lapse CSEM surveying. The CSEM method is sensitive to the presence of fluids in the pore space, including resistive $CO_2$, offering the possibility to complement industry 4D-seismic surveying and quantify the volume of the $CO_2$ in the reservoir.

## Acknowledgements

The study is performed with support from the Research Council of Norway (CLIMIT-KPN 295212) and the NCCS Centre (NFR project number 257579/E20), performed under the Norwegian research program Centres for Environment-friendly Energy Research (FME).

## References

Amaya, M., Morten, J. P., & Boman, L. (2016): A low-rank approximation for large-scale 3D controlled-source electromagnetic Gauss-Newton inversion. Geophysics, 81(3), E211-E225.

Archie, G.E. (1942): The electrical resistivity log as an aid in determining some reservoir characteristics. Petroleum Transactions of AIME. 146: 54–62.

Bøe, L. Z., Park, J., Vöge, M., & Sauvin, G. (2017). Filtering out seabed pipeline influence to improve the resistivity image of an offshore $CO_2$ storage site. In EAGE/SEG Research Workshop.

Colombo, D. and McNeice, G. W. (2013): Quantifying surface-to-reservoir electromagnetics for waterflood monitoring in a Saudi Arabian carbonate reservoir, GEOPHYSICS, 78:6, E281-E297

Constable, S. C., Parker, R. L., Constable C. G. (1987): Occam's inversion: a practical algorithm for generating smooth models from electromagnetic sounding data. Geophysics, 52(3): 289–300.

Dupuy, B., Torres, V., Romdhane, A., & Ghaderi, A. (2018, October). Norwegian large-scale CO2 storage project (Smeaheia): baseline geophysical models. In 14th Greenhouse Gas Control Technologies Conference Melbourne (pp. 21-26).

Eliasson, P., & Romdhane, A. (2017, June). Uncertainty Evaluation in Waveform-based Imaging Methods-A Case Study at Sleipner. In 79th EAGE Conference and Exhibition.

Gassnova (2016). Feasibility study for full-scale CCS in Norway. Technical report, Gassnova.

Gehrmann, R. A., Haroon, A., Morton, M., Djanni, A. T., & Minshull, T. A. (2020): Seafloor massive sulphide exploration using deep-towed controlled source electromagnetics: Navigational uncertainties. Geophys. J. Int., *220*(2), 1215-1227.

Grayver, A. V., Streich R. and Ritter O. (2014): 3D inversion and resolution analysis of land-based CSEM data from the Ketzin CO2 storage formation, Geophysics, 79:2, E101-E114

Halko, N., Martinsson, P. G., & Tropp, J. A. (2011): Finding structure with randomness: Probabilistic algorithms for constructing approximate matrix decompositions. SIAM review, 53(2), 217-288.

Key, K. and Ovall, J. (2011): A parallel goal-oriented adaptive finite element method for 2.5-D electromagnetic modelling. Geophys. J. Int., 186, 137-154.

Key, K. (2016): MARE2DEM: a 2-D inversion code for controlled-source electromagnetic and magnetotelluric data. Geophys. J. Int., 207(1), 571-588.

Lien, M., & Mannseth, T. (2008): Sensitivity study of marine CSEM data for reservoir production monitoring. Geophysics, 73(4), F151-F163.

Lothe, A. E., Bergmo, P. E. S., Emmel, B., & Eliasson, P. (2018, October): Effects of uncertainties in fault interpretations on pressure depletion and $CO_2$ storage injection at Horda Platform, offshore Norway. In 14th Greenhouse Gas Control Technologies Conference Melbourne (pp. 21-26).

Maurer, H. R.,D. E. Boerner, and A. Curtis, 2000, Design strategies for electromagnetic geophysical surveys: Inverse Problems, 16(5), 1097–1118.

Maurer, H., Curtis, A., & Boerner, D. E. (2010) : Recent advances in optimized geophysical survey design. Geophysics, 75(5), 75A177-75A194.

Morten, J. P., & Bjørke, A. (2020): Imaging and Quantifying $CO_2$ Containment Storage Loss Using 3D CSEM. In 82nd EAGE Annual Conference & Exhibition, 2020(1), 1-5. European Association of Geoscientists & Engineers.

Mulrooney, M. J., Osmond, J. L., Skurtveit, E., Faleide, J. I., & Braathen, A. (2020): Structural analysis of the Smeaheia fault block, a potential $CO_2$ storage site, northern Horda Platform, North Sea. Marine and Petroleum Geology, 121, 104598.

Orange, A., Key, K., & Constable, S. (2009). The feasibility of reservoir monitoring using time-lapse marine CSEM. Geophysics, 74(2), F21-F29.

Park, J., Bjørke, A. K., Sauvin, G., Morten, J. P., & Nazarian, B. (2019): Marine CSEM for $CO_2$ Storage Monitoring-North Sea Sensitivity Study. In 81st EAGE Conference and Exhibition 2019(1), 1-5. European Association of Geoscientists & Engineers.

Patzer, C., Ritter, O., & Tietze, K. (2017). Time-lapse CSEM inversion using focusing regularization techniques for reservoir monitoring. In SEG Technical Program Expanded Abstracts (pp. 5870-5874). Society of Exploration Geophysicists.

Romdhane A, Eliasson P. Optimized Geophysical Survey Design for $CO_2$ Monitoring–A Synthetic Study. In14th Greenhouse Gas Control Technologies Conference Melbourne 2018 Oct (pp. 21-26).

Roux, E., & García, X. (2014): Optimizing an experimental design for a CSEM experiment: methodology and synthetic tests. Geophys. J. Int., 197(1), 135-148.

Shantsev, D. V, Nerland, E. A. and Gelius, L.-J., (2020): Time-lapse CSEM: how important is survey repeatability?, Geophys. J. Int., 223(3), 2133–2147.

Streich, R. (2016). Controlled-source electromagnetic approaches for hydrocarbon exploration and monitoring on land. Surveys in geophysics, 37(1), 47-80.

Tietze, K., Ritter, O., Patzer, C., Vesken, P., Dillen, M. (2019): Repeatability of land-based controlled-source electromagnetic measurements in industrialized areas and including vertical electric fields. – Geophys. J. Int., 218(3), pp. 1552—1571

Zach, J. J., Frenkel, M. A., Ostvedt-Ghazi, A. M., De Lugao, P., & Ridyard, D. (2009, August). Marine CSEM methods for 3D hydrocarbon field mapping and monitoring. In 11th International Congress of the Brazilian Geophysical Society & EXPOGEF 2009, Salvador, Bahia, Brazil, 24-28 August 2009 (pp. 480-485). Society of Exploration Geophysicists and Brazilian Geophysical Society.